



## A positive radiative-dynamic feedback mechanism for the maintenance and growth of Martian dust storms

Scot C. R. Rafkin<sup>1</sup>

Received 5 June 2008; revised 10 September 2008; accepted 5 November 2008; published 30 January 2009.

[1] Atmospheric dust disturbances ranging in size from dust devils to planet-encircling dust storms are ubiquitous on Mars. After dust devils, the most common disturbances are local- or regional-scale disturbances. The origin of some of these mesoscale systems has been previously investigated and found to be linked to lifting along frontal systems or cap edge circulations. Very little attention has been given to whether the lifted dust in these systems result in radiative forcing that might modulate the local system dynamics with an amplitude large enough to affect local dust-lifting processes. Idealized numerical modeling results presented herein show that a positive feedback process between local dynamics and radiative forcing of lifted dust can occur under some conditions. The feedback process is distinctly different than an enhancement of the general circulation by increasing atmospheric dust loading because the dynamical effects of this feedback process occur locally, within the disturbance itself. Optimal conditions for growth of initial atmospheric dust perturbations include (1) subtropical latitudes associated with relatively large solar insolation and moderate coriolis force; (2) modest dust-lifting thresholds and dust-lifting efficiencies; (3) relatively large initial dust perturbations; (4) steep background lapse rates; and (5) a barotropic environment. The positive feedback process is explained by a combination of geostrophic adjustment theory and a Carnot engine-like mechanism related to the Wind-Induced Sensible Heat Exchange hypothesis for tropical cyclones on Earth.

**Citation:** Rafkin, S. C. R. (2009), A positive radiative-dynamic feedback mechanism for the maintenance and growth of Martian dust storms, *J. Geophys. Res.*, 114, E01009, doi:10.1029/2008JE003217.

### 1. Introduction

[2] Atmospheric dust plays an important role in regulating the climate of Mars and strongly influences the deposition of incoming solar energy and outgoing infrared radiation, thereby affecting atmospheric dynamics through heating. Therefore, the atmospheric dust cycle is intrinsically a key element to understanding the weather and climate system of Mars, including stochastic dust storms. The lifting of dust from the surface is fundamentally a result of atmospheric circulations, and since the lifted dust can radiatively influence the atmospheric dynamics, there exists the potential for feedback between atmospheric dynamics, dust-lifting processes, and the radiative forcing perturbations that ensue. The plausibility and nature of this feedback is addressed in this paper.

[3] Dynamical atmospheric instabilities resulting from radiatively active atmospheric dust have been previously recognized. *Gierasch et al.* [1973] forwarded theoretical arguments for dynamical instabilities arising from a horizontally extensive aerosol layer under the condition that the infrared radiative heat flux in the layer is dependent on the

height of the layer. Later, *Ghan* [1989] considered solar heating of horizontally extensive aerosol layers, and provided theoretical arguments indicating that the radiative effects of atmospheric dust could result in a kinetic energy growth rate comparable to that of baroclinic instability. Two modes of instability (propagating and advective) were identified, and the condition for the instability was the presence of a vertical gradient of aerosol mixing ratio. *Haberle et al.* [1982] demonstrated that atmospheric dust loading similar to that expected in planet-encircling dust storms could accelerate the zonal mean flow.

[4] None of these previous studies included the process of dust lifting from the surface into the atmosphere, and there was no direct investigation of whether the disturbances were capable of maintaining or enhancing the dynamically unstable atmospheric dust distribution through the replenishment of airborne dust from the surface. Furthermore, none of these studies investigated the instabilities or feedbacks that might result from horizontally finite dust disturbances from which any effectively horizontally infinite or global dust distribution must originate.

[5] *Gierasch and Goody* [1973] applied the theoretical hurricane model of *Carrier* [1971] to a hypothetical Mars dust storm to predict the time-dependent depth and intensity based on diurnally varying heating. Growth of the system was dependent on the initial depth, vertical core velocity and swirl velocity. As in previous studies, feedback from

<sup>1</sup>Department of Space Studies, Southwest Research Institute, Boulder, Colorado, USA.

additional dust lifted into the system was not considered, although the importance of reaching a saltation threshold was recognized.

[6] More recent general circulation modeling studies [Kahre *et al.*, 2006; Basu *et al.*, 2006] have included dust-lifting parameterizations tied directly to the atmospheric wind stress and atmospheric lapse rate. The results of these investigations show that the atmospheric dust loading is sensitive to the choice of free parameters within the lifting parameterization; the models can generate regional dust storms and even planet-encircling dust storms with suitably tuned parameter values. In the simulations by Basu *et al.*, rapid growth of planetary-scale dust storms was linked directly to the intensification of the Hadley Cell. Wang [2007] also found that large dust storms strengthen the Hadley Cell circulation while suppressing transient baroclinic eddies. However, these studies did not investigate the possible interplay between atmospheric dust, local atmospheric dynamics, and dust lifting. Does the lifted dust lead to amplification of the local circulation producing the initial dust lifting (as opposed to an amplification of the large-scale mean circulation)? Or, is the lifted atmospheric dust primarily passive, revealing only the presence of an atmospheric circulation while contributing little to its dynamical forcing? Toigo *et al.* [2002], in investigating dust storms along the polar cap edge, did explore the possibility of a modulated surface wind stress due to radiative-dynamic feedback and found little evidence for such an effect.

[7] A number of three-dimensional numerical simulations designed to investigate a possible radiative-dynamic dust feedback mechanism, operating at local rather than global scales, are presented in this study. Briefly, the potential positive feedback mechanism works as follows: (1) wind lifts dust from the surface into the atmosphere; (2) the increased atmospheric dust load results in increased radiative heating of the atmosphere during the day, or less radiative cooling during the night, thereby producing a relatively warm region on the scale of the lifted dust; (3) surface pressure is hydrostatically lowered in the warm region, which leads to an amplification of the low-level pressure gradient force; (4) the increased pressure gradient results in stronger winds, which lift more dust, and thus completes the positive feedback loop. The model simulations are designed to answer the following questions: Does a feedback exist, and if so, under what circumstances? How sensitive is the mechanism to various initial conditions and variations in the dust-lifting process? Is this mechanism consistent with any observed dust disturbances and where and when might a feedback-driven storm be observed?

## 2. Approach and Numerical Experiment Design

[8] The basic approach to identify the presence and strength of a potential feedback mechanism is to conduct simplified numerical simulations in which the lifting of dust is switched on and off. Simulations in which no dust lifting is allowed represent control cases that short-circuit the potential feedback process. Under otherwise identical conditions and forcing, the “on” simulations can be compared to the “off” simulations to see whether the ability of the atmosphere to lift dust produces a more energetic, robust, or dynamically stronger system than in the case where no dust

lifting is permitted. Further experimentation with dust-lifting parameters, coriolis force, latitude, solar heating, and initial conditions are conducted to assess the impact on the feedback.

### 2.1. Model Description

[9] The Mars Regional Atmospheric Modeling System (MRAMS) is employed for these studies, with the core of the model as described by Rafkin *et al.* [2001]. However, in this study, we couple the dynamical MRAMS model to the Cloud Aerosol and Radiation Model for Atmospheres (CARMA) as described by Michaels *et al.* [2006] to achieve a more physically realistic representation of dust and dust processes that are at the core of the proposed feedback cycle.

[10] MRAMS/CARMA distributes atmospheric dust into eight discrete mass bins. Each dust bin is carried in the model as an individual scalar quantity that is both advected, and diffused, and each dust bin undergoes mass-dependent sedimentation. All atmospheric dust is radiatively active, and heating rates are calculated on the basis of the two-stream correlated k model of Toon *et al.* [1989].

[11] Dust lifting, when activated, is parameterized according to Kahre *et al.* [2006]

$$F_{dust} = \alpha \tau^2 (\tau - \tau_c) / \tau_c, \quad (1)$$

where  $\tau_c$  is the critical surface stress (lifting threshold) above which dust lifting is allowed, and  $\alpha$  determines the total flux of dust lifted. The lifted dust is assumed to follow a lognormal distribution with a mode of approximately  $1 \mu\text{m}$ .

### 2.2. Model Domain Configuration

[12] The simulations presented in this paper are idealized. The surface is horizontally homogeneous with an albedo of 0.2 and a thermal inertia of  $385 \text{ J m}^{-2} \text{ K}^{-1} \text{ s}^{-1/2}$ . The model is started with the atmosphere at rest, but the background dust is perturbed in the center of the model domain to initiate a disturbance. The perturbation is of variable horizontal size, but is  $\sim 200 \text{ m}$  deep with an optical depth of 1.0. The model is integrated in time for approximately three sols.

[13] The model domain is sufficiently large ( $>10^3 \text{ km}$  across) such that the circulations of interest in the center of the domain are insensitive to the boundaries or choice of boundary conditions. Test simulations and previous studies [e.g., Michaels and Rafkin, 2004] indicate that organized convective structures at scales of (O)10 km are present in the convective boundary layer. Dust-lifting variability is expected to follow the scale of wind variability associated with these structures, but it is not computationally possible to have a grid with  $10^3$  points on a side. Instead, nested grids with the following dimensions and grid spacing are used:  $40 \times 40$  at 64 km (grid 1);  $62 \times 62$  at 16 km (grid 2);  $50 \times 50$  at 4 km (grid 3);  $101 \times 101$  at 1.33 km (grid 4). There are 40 sigma-z vertical points that are geometrically stretched by a factor of 1.18 from an initial spacing of 15 m to a maximum of 3000 m, resulting in a model top at 50 km. Grid 4 is sufficient to capture much of the convective structure where dust lifting is occurring, while the parent grids capture the mesoscale dynamics resulting from the heating of the lifted dust. In most cases, the bulk of the disturbed circulation that develops is confined to the third

**Table 1.** Summary of Simulations

Simulation Identifier	Coriolis	Initial Dust Radius (km)	Initial Temperature Profile (K)	Dust-Lifting Configuration
S0 (control)	$f$ plane	10	170	lifting off
S1	$f$ plane	10	170	$\tau = 14$ mN, $\alpha = 7 \times 10^{-4}$ s <sup>3</sup> m <sup>2</sup>
S2	$f$ plane	10	170	$\tau = 1$ mN, $\alpha = 7 \times 10^{-4}$ s <sup>3</sup> m <sup>2</sup>
S3	$f = 0$	10	170	lifting off
S4	$f$ plane	10	215	$\tau = 1$ mN, $\alpha = 7 \times 10^{-4}$ s <sup>3</sup> m <sup>2</sup>
S5	$f$ plane	10	realistic	$\tau = 1$ mN, $\alpha = 7 \times 10^{-4}$ s <sup>3</sup> m <sup>2</sup>
S6	$f$ plane	10	170	$\tau = 14$ mN, $\alpha = 1 \times 10^{-2}$ s <sup>3</sup> m <sup>2</sup>
S7	$f$ plane	50	170	$\tau = 14$ mN, $\alpha = 7 \times 10^{-4}$ s <sup>3</sup> m <sup>2</sup>

grid, although weak circulations and gravity waves do extend out into the parent grids. The perturbations of pressure and wind at the edge of the outermost grid are extremely small, indicating that the effects of the disturbances and circulations occurring in the center of the domain are well contained. Test simulations with slightly smaller domains and variable lateral boundary conditions confirmed that the results are insensitive to the domain size and choice of boundary condition.

### 2.3. Free Parameters

[14] A number of parameters that might be expected to influence the putative feedback mechanism are explored independently and in combination. These parameters include (1) horizontal dimension of the initial dust disturbance; (2) solar flux; (3) coriolis force via changes in latitude; (4) background thermodynamic structure of the atmosphere; and (5) variations of the two independent variables representing dust-lifting processes (equation 1). It was not possible to explore the full space of parameter combinations. However, the simulations that were undertaken were judiciously selected and the range of results is sufficient to reasonably characterize the response of the atmosphere to changes in the various parameters.

## 3. Results

[15] Three-dimensional simulations relevant to subsequent discussion are shown in Table 1. In all of the studies, a full solar cycle was imposed with the simulation starting at sunrise at  $L_s = 180^\circ$ . The incident solar flux depends on latitude, and the simulations use an  $f$  plane (constant coriolis parameter) approximation with a value corresponding to the solar flux latitude. The coriolis force was switched off ( $f = 0$ ) in some cases with nonzero latitudes.

[16] Quantitative measures are required to assess feedback amplitude. Several parameters, including minimum central pressure, domain-averaged or domain-integrated surface wind speed, and total domain kinetic energy, were calculated for this purpose. All of these quantities provided consistent identification of the intensity of any feedback signal. For example, there was a one-to-one correspondence between surface wind speed and the central pressure deficit. In most cases, the circulation that developed was almost entirely contained within the third grid during the simulation, and thus feedback parameters may be meaningfully computed on this grid or its parents.

### 3.1. Effect of Coriolis Force and Solar Forcing

[17] Latitude controls both solar insolation and the coriolis parameter. Figure 1 displays the minimum central pressure on grid 1 as a function of latitude and time for the control simulation (S0). Simulation S0 does not have active dust lifting; only the dust perturbation at initialization is present and this dust is free to advect, diffuse, and sediment. Therefore, the results represent the response of the atmosphere to dust loading without the possibility of the system producing a feedback (positive or negative), and only the response of the atmosphere to the initial dust perturbation is simulated. The overall downward trend for each latitude is due to the warming of the atmosphere over time from the initial 170 K isothermal state. The diurnal heating cycle produces the pressure oscillations on top of the downward trend, and the amplitude of the cycle is approximately the same for each sol. At  $L_s = 180$ , all latitudes receive 12 h of daylight, and thus the pressure cycles for all latitudes are in phase. The pressure signals at latitude 0, 15, and 30 degrees are similar, although the 15° case has the lowest minimum pressure.

[18] Solar insolation alone should induce a monotonic increase in minimum pressure as a function of increasing latitude, with the magnitude of the depression tied directly to a hydrostatic pressure decrease resulting from warming of the atmospheric column containing dust. That S0 does not show this trend indicates that there are dynamical forces at play. This is not entirely unexpected, as the idealized simulations are one manifestation of the classic geostrophic adjustment problem.

[19] To better illustrate this, consider an infinite, homogeneous, incompressible shallow fluid initially at rest (this example is based on a homework exercise assigned by Richard Johnson at Colorado State University). The system is rotating with nonzero angular velocity  $\Omega$  with depth  $H$ . The surface is displaced in the region  $a \leq x \leq a$  by a height  $\Delta H$  at  $t = 0$ . At  $t \rightarrow \infty$ , the shallow water system is in steady state geostrophic flow where the pressure (height) field is balanced by the coriolis force. Prior to this balance, the system undergoes a geostrophic adjustment process through the radiation of energy via buoyancy oscillations (gravity waves). The fraction of the initial available energy radiated away in gravity waves at the final state is

$$\frac{E_g}{P_o} = \frac{\lambda_R}{2a} \left(1 - e^{-2a/\lambda}\right), \quad (2)$$

## Minimum Domain Pressure Simulations S0 and S1

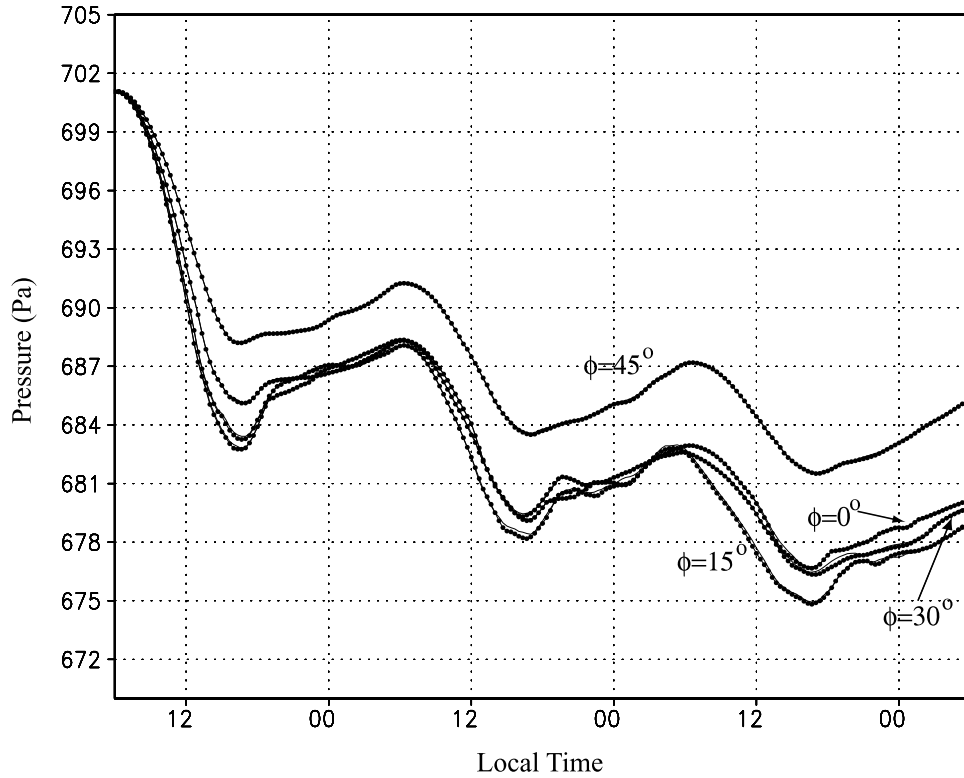


**Figure 1.** Grid 1 domain minimum pressure as a function of time for simulation S0 (solid lines) and S1 (solid lines with circles) shows the influence of solar insolation and dynamics at the indicated latitudes. Although dust lifting is allowed in S1, the results between the two simulations are almost indistinguishable because the circulation that develops is generally too weak to lift dust. The pressure deficit in the subtropical cases is greatest because of optimal juxtaposition of heating and dynamical response. The equatorial case lacks a geostrophic adjustment process while the middle latitude case suffers from decreased solar forcing.

where  $E_g = P_o - E_f$ ,  $P_o$  is the initial available potential energy (all potential energy),  $\lambda_R$  is the Rossby Radius of Deformation given by  $\lambda_R = \sqrt{gH}/f$ , and  $E_f$  is the total energy (kinetic plus potential) in the final state.

[20] If  $a \ll \lambda_R$  then the fraction of energy radiated is approximately one. Therefore, for disturbances that are small compared to the Rossby Radius of Deformation, nearly all the energy is lost from the system and very little energy remains for a balanced geostrophic flow. The final state of the system under this condition is a nearly flat surface (near-zero potential energy) with little motion (near-zero kinetic energy). In other words, the system tends to return to its initial state; the mass (pressure) field adjusts to the initial kinematic state. For low latitudes,  $\lambda_R$  is quite large owing to the small coriolis parameter. Thus, the typical response of the tropical atmosphere to a disturbance is the emanation of gravity waves that flatten the pressure field, with a corresponding decrease in winds.

[21] In contrast to the tropics, the Rossby Radius of Deformation can be much smaller than the disturbance in the subtropics and middle latitudes. In this situation ( $a \gg \lambda_R$ ), the fraction of energy radiated as gravity waves is approximately zero. All the energy remains in the system, with no adjustment of the mass (pressure) field. Instead, the winds

increase to geostrophically balance the initial pressure disturbance.

[22] Another way to interpret this result is to consider the time scale of gravity wave propagation and the time scale over which the coriolis force operates: the Rossby Radius of Deformation is the ratio of the gravity wave phase speed to the vorticity. As gravity waves propagate outward, gravity waves suffer a coriolis torque and are trapped at distances less than the Rossby Radius of Deformation. Therefore, as the coriolis parameter increases, the Rossby Radius of Deformation decreases, and the energy generated at the center of the disturbance is confined to a smaller region. The result is the development of a quasi-balanced circulation dominated by geostrophic balance (or gradient wind balance when accounting for surface friction). Once a circulation develops, a further local decrease in the Rossby Radius of Deformation will occur as the relative vorticity contributes analogously to planetary vorticity.

[23] Despite the largest solar forcing at the equator, the equatorial S0 simulation is not the lowest pressure case because the mass field is constantly adjusting to fill in the pressure deficit (via gravity waves). At 15°, the solar forcing is slightly less than at the equator, but the conversion of some of the solar energy to kinetic energy as part of

## Pressure and Wind Simulation S0

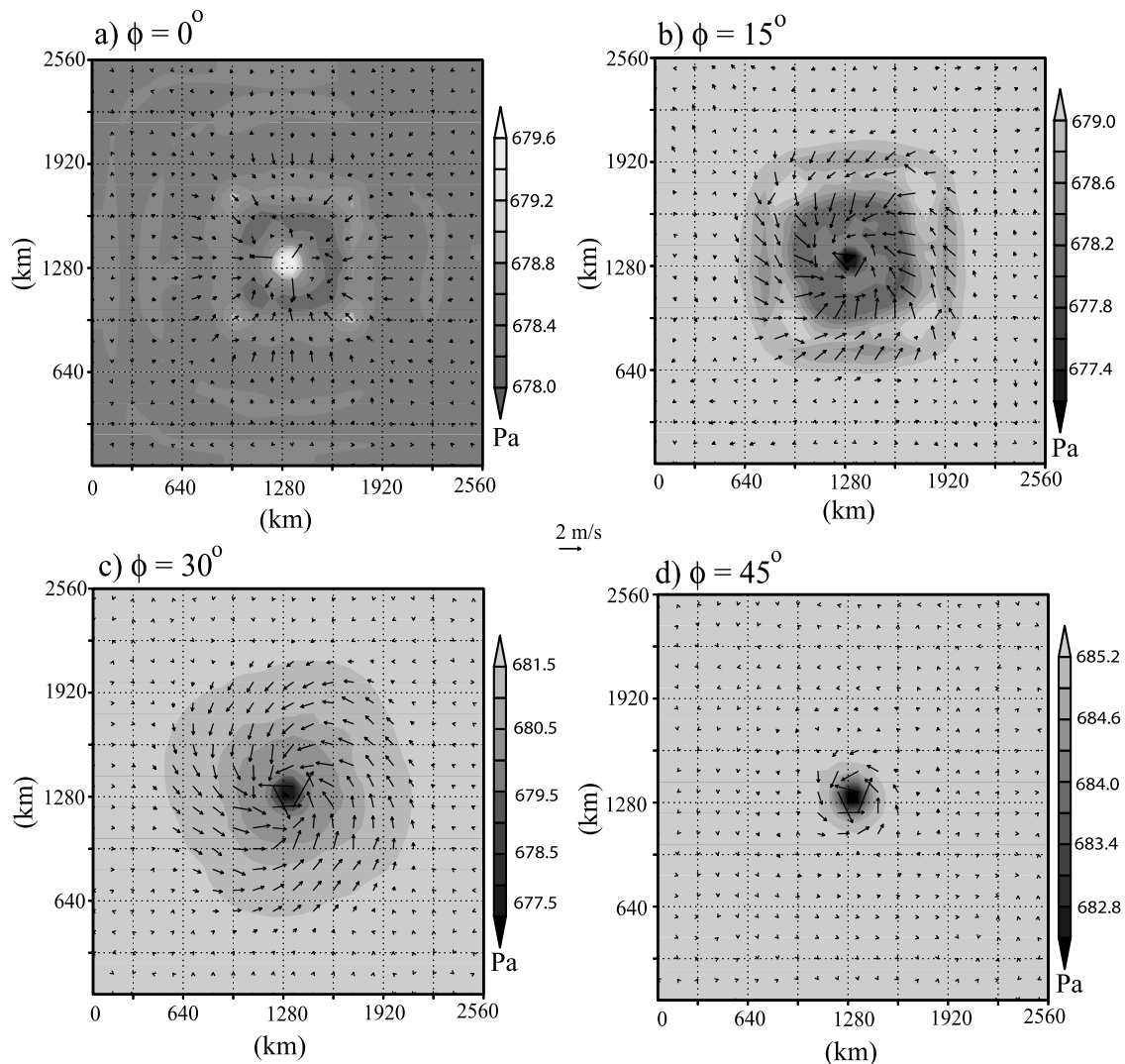


**Figure 2.** Horizontal cross sections of the winds and pressure field at the lowest model level of simulation S0 illustrate the dynamical differences associated with latitudes of (a)  $0^\circ$ , (b)  $15^\circ$ , (c)  $30^\circ$ , and (d)  $45^\circ$ . Gravity wave oscillations are most apparent in the equatorial case, including evidence of a transient local pressure maximum at the center of the disturbance. Gravity wave energy becomes less obvious with increasing latitude, while the balanced circulation component becomes increasingly dominant. A  $2 \text{ m s}^{-1}$  reference wind vector is located in the center. The data are approximately 53 h into the simulation.

a geostrophically balanced circulation permits some of the mass to remain in a pressure deficit configuration. The dynamics at this latitude slightly counteract the decrease in solar forcing and result in a slightly more intense system than at the equator. At  $15^\circ$ , the Rossby Radius of Deformation is still quite large (although not infinite as in the equatorial case), so the dynamic contribution to the pressure deficit is relatively small, but still large enough to exceed the equatorial case. The model solution at  $30^\circ$  nearly matches the equatorial case even though there has been a further reduction in solar heating. Here, the dynamic response is stronger than at  $15^\circ$ , but the solar forcing is less. At  $45^\circ$  the loss of solar insolation begins to overwhelm

the increasing tendency to develop a more geostrophically balanced system. Correspondingly, the pressure deficit is less than at the lower latitudes.

[24] Examination of horizontal cross sections in the late afternoon in the third sol of the control simulation further illustrates the influence of dynamical processes at different latitudes (Figure 2). At the equator, gravity waves perturb both the pressure and wind field. Although the pressure decreases toward the center of the disturbance on average, the central pressure is actually slightly higher, as a result of oscillating wave activity, at the instant of time shown in Figure 2. A short time later (and prior), the pressure in the center is at a domain minimum. The winds are convergent/

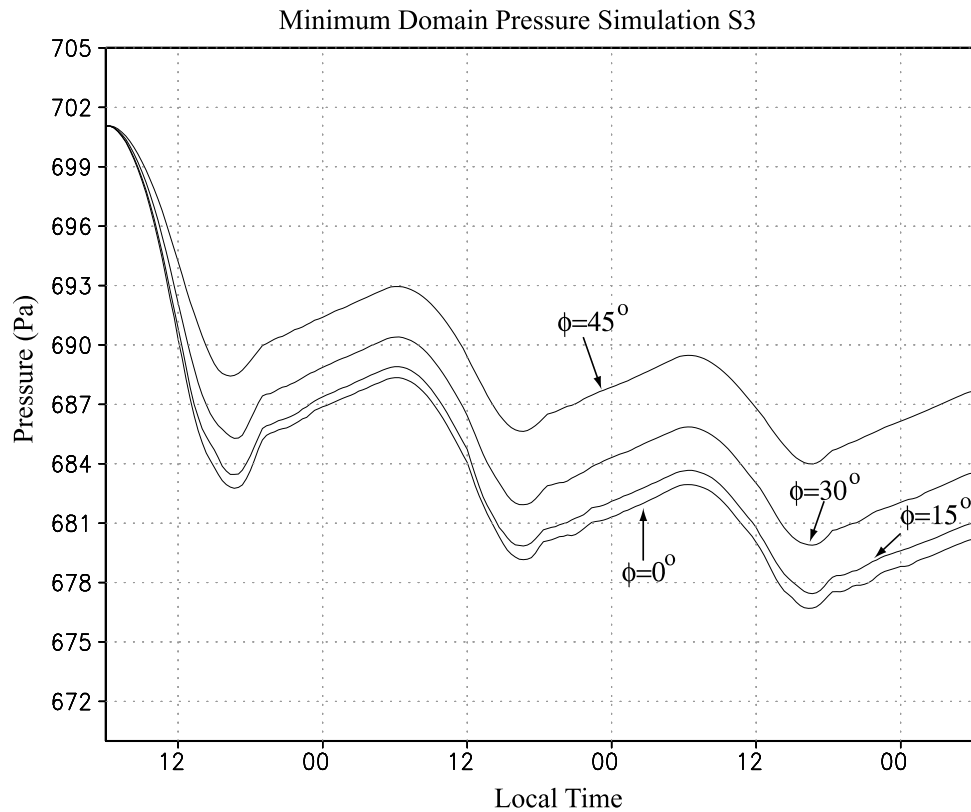


**Figure 3.** Without a geostrophic adjustment process (simulation S3), the grid 1 domain minimum pressure decreases as a function of solar insolation.

divergent in response to the pressure field, and there is no rotation, as expected. Viewed in time, the equatorial simulation resembles the response of the surface of a pond disturbed by a rock. At a latitude of  $15^\circ$ , there is still evidence of gravity waves in the pressure field, but much less so than at  $0^\circ$ . The central pressure is at a domain minimum and remains that way throughout the simulation. The winds have a notable rotational (geostrophic) component, but there are locations, particularly where the pressure gradient is strongest, where the winds cross the isobars at nearly right angles. By  $30^\circ$  latitude, rotational dynamical processes are clearly evident. There is no obvious evidence in either the pressure or wind field of gravity waves propagating within the domain. The winds are clearly rotational and the corresponding pressure field is relatively smooth with a sharp gradient of pressure near the central minimum. At  $45^\circ$  the system has become quite compact, with pressure perturbations greatest very near the center and a nearly flat pressure field elsewhere. Gravity wave evidence is completely absent. Although the dynamic environment is conducive to maintenance of a compact and intense circulation, the decreased solar forcing limits the intensity. Comparing the results from all latitudes, the  $15^\circ$  and  $30^\circ$  cases are the most intense in terms of pressure deficit, wind speeds, and overall organization.

[25] Experiment S3 (Figure 3) isolates the influence of solar insolation by forcing the coriolis parameter to zero for all latitudes, but is otherwise identical to S0. Under these conditions, no geostrophic adjustment is possible. The equatorial case is now the deepest, followed by  $15^\circ$ ,  $30^\circ$ ,

and finally  $45^\circ$ . The differences between S0 and S3 are strictly due to differing dynamical responses associated with the geostrophic adjustment process. The  $15^\circ$  S3 case is only slightly weaker compared to S0 because the dynamical impact at this latitude is still relatively small. The greatest impact is in the  $30^\circ$  and  $45^\circ$  cases where the coriolis force would normally play a larger role.

[26] On the basis of simulations S0 and S3, the atmospheric response to an initial dust loading perturbation is a decrease in surface pressure at the location of the dust. The decrease in pressure is maximized near  $15^\circ$  where the system benefits from relatively high values of solar insolation and a decreasing Rossby Radius of Deformation. At latitudes below  $\sim 15^\circ$  the dynamical environment is not favorable for the development of balanced vortical motion, and, in the absence of solar forcing, the overall tendency is for the tropical atmosphere to return to a motionless, unperturbed state via the export of energy by gravity waves. Between about  $15^\circ$ – $30^\circ$  latitude, where favorable solar forcing and dynamical conditions are found, the most robust systems are likely to be found. At higher latitudes, the dynamical environment is highly favorable for the development of an intense compact system, but the energy input is inadequate. Therefore, with all other things being equal, dust disturbances are most likely to produce a noticeable atmospheric perturbation in the tropics and subtropics. This is not to say that high-latitude dust disturbances are not possible, but rather that they are less likely to produce a significant feedback with the dynamics.

## Minimum Domain Pressure Simulations S0 and S2

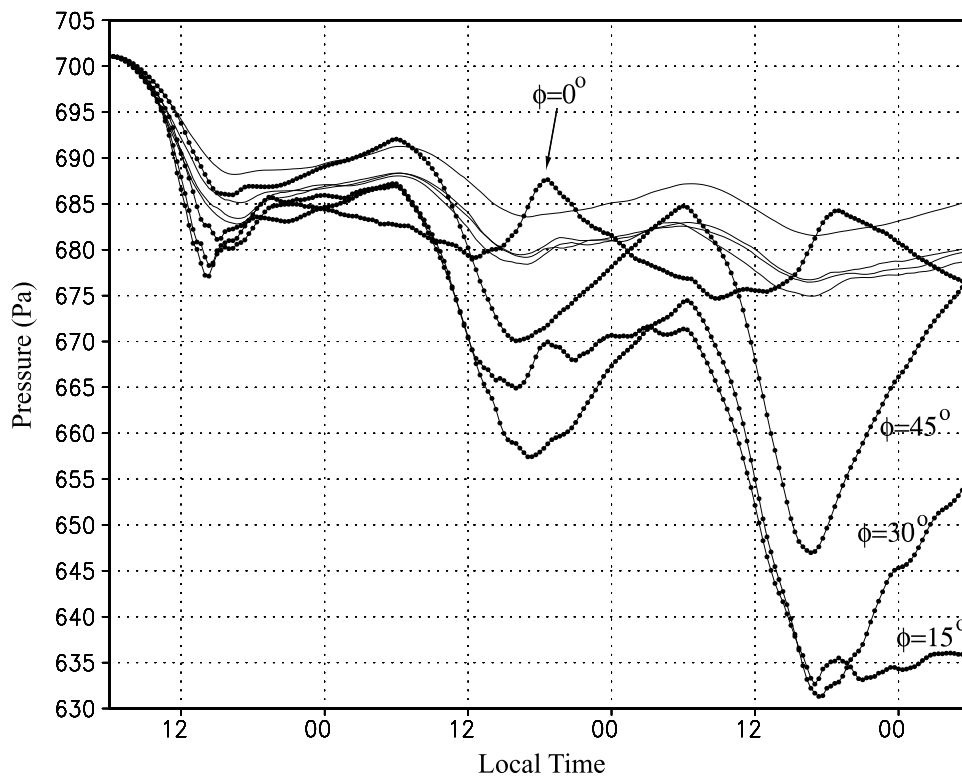


**Figure 4.** Grid 1 domain minimum pressure for simulation S0 (solid lines) and S2 (solid lines with circles) shows the positive feedback when the dust-lifting threshold is lowered to a relatively small value. The feedback is optimized in the subtropics and is almost nonexistent at the equator. The data are approximately 53 h into the simulation.

### 3.2. Effect of Dust-Lifting Parameters

[27] Three variations of the control experiment are designed to test the effects of dust-lifting parameters. S1 and S2 allow lifting of radiatively active dust by the atmospheric circulation. The former uses “standard” dust-lifting values for both the lifting threshold and lifting efficiency. The latter uses a highly reduced threshold that allows the circulation to much more easily lift dust.

[28] The control case, S0, and the dust-lifting case S1 are nearly identical (Figure 1). This is the result of wind speeds being generally insufficient to lift dust. S0 wind speeds are typically less than  $10 \text{ m s}^{-1}$ . Notably, the  $15^\circ$  S1 simulation, which has the greatest wind speeds, shows the most deviation from S0. However, without much lifted dust, S0 and S1 evolve in a similar manner.

[29] When the dust-lifting threshold is reduced, as in S2, the situation is much different (Figure 4). At all latitudes, except for the equator, the mean pressure in S2 is substantially lower than S0 (or S1). In S2 compared to S0 or S1, there is less of a nocturnal pressure rise to compensate for the decrease during the day, indicating that the system is strengthening each sol. Corresponding with the lower pressure is an almost twofold increase in wind speed and a concomitant increase in kinetic energy compared to S0 (Figure 5). Therefore, S2 exhibits a positive feedback (except at the equator) whereby the initial dust distribution produces a pressure depression that accelerates the winds. These winds then lift and entrain additional dust that further

reduces the pressure and increases the wind (Figure 6). The greatest lifting is associated with the strongest winds in Figure 6, and the lifting is nearly collocated with the highest opacity.

[30] The importance of developing a dynamically balanced system distinguishes the middle latitudes and subtropics from the tropical latitudes in the case of positive feedback (S2). Unlike the control case where simulations at latitudes less than  $30^\circ$  all showed pressure depressions, the S2 simulations show that the most rapidly deepening and self-amplifying disturbances are most likely to be found in the subtropics where there is an optimal juxtaposition of solar heating and coriolis force. At the equator, energy propagates away from the core of the disturbance and the pure irrotational circulation is unable to focus or organize the atmospheric dust, regardless of the ease of dust lifting (Figure 6). Overall, there is little difference in pressure between S0, S1, and S2 for the equatorial case, except that the amplitude of the diurnal pressure signal is larger for S2. With respect to dust, the dust optical depth at the equator decays from the initial  $\tau = 1$ , but does so more slowly in S2. Also, there is a net convergence of dust toward the center of the circulation in S2.

[31] In contrast, the S2 subtropical disturbances have a vortex that helps retain energy and keep the lifted dust focused in the core of the system. Indeed, the low-level circulation tends to transport dust lifted at the periphery toward the center. The subtropical cases are much deeper

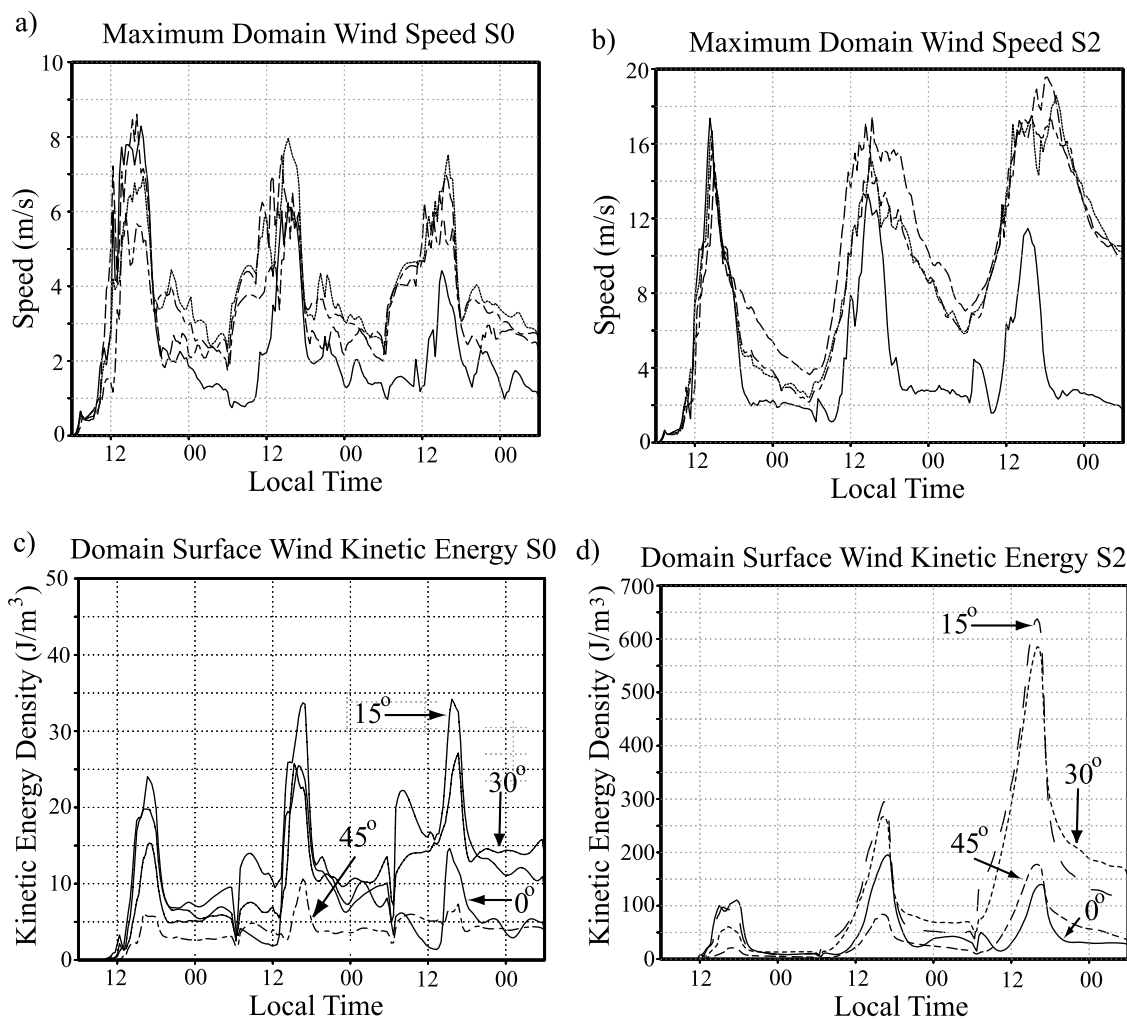


**Figure 5.** Corresponding to the pressure falls associated with the positive feedback in S2 (Figure 4), there is a dramatic increase in the maximum wind speed and kinetic energy at the surface. In all plots the solid line is  $0^\circ$ , long dashed line is  $15^\circ$ , short dashed line is  $30^\circ$ , and long-short dashed line is  $45^\circ$ . For comparison, kinetic energy from S0 is also shown. At the equator, the system in S2 has lower wind speeds and kinetic energy on the third sol compared to the second, indicating a lack of positive feedback. The size of the disturbances decrease with increasing latitude, and this results in much greater energy for the  $15^\circ$  and  $30^\circ$  latitude cases.

than in the control case. Finally, the  $45^\circ$  latitude case also shows considerable feedback, with dust optical depths comparable to the  $15^\circ$  case, although the kinetic energy is less.

[32] The development of a balanced circulation is important not only to the magnitude of the feedback process, but also to the longevity of the disturbance after sunset, when the source of energy is removed. A balanced circulation is dynamically “stiffer” than unbalanced circulations. Simulations that exhibit little to no organized vorticity by the end of the first sol rapidly dissipate (via gravity wave propagation and frictional spin down) and are not able to redevelop on subsequent sols (e.g.,  $0^\circ$  latitude in S2). On the other hand, in those simulations where a vortex is present, it may remain through the night and provide a focus for reintensification on the next sol. Such a persistent circulation may also continue to lift dust during the night, will have a tendency to keep the dust aloft owing to organized upwell-

ing at the center, and will tend to keep the dust concentrated near the center. However, wind speeds and lifting decrease over night in even the strongest storms. In weaker systems, dust lifting may completely cease during the night. Disturbances that spin down overnight tend to have a more diffuse and widespread dust distribution that does not provide a good focusing mechanism at sunrise on the following sol. Note that the pressure rises during the night hours are much less than the pressure falls during the day for the  $15^\circ$  and  $30^\circ$  cases in S2. This allows the system to continue deepening on subsequent sols. In particular the  $15^\circ$  case, with only a slight increase in nocturnal pressure, seems to be on a runaway positive feedback trajectory (Figure 4).

[33] The proper value of lifting threshold appropriate for Mars is unknown, and almost certainly is a function of the properties of the surface. It is also known to be a function of model resolution, and most likely, the choice of model.

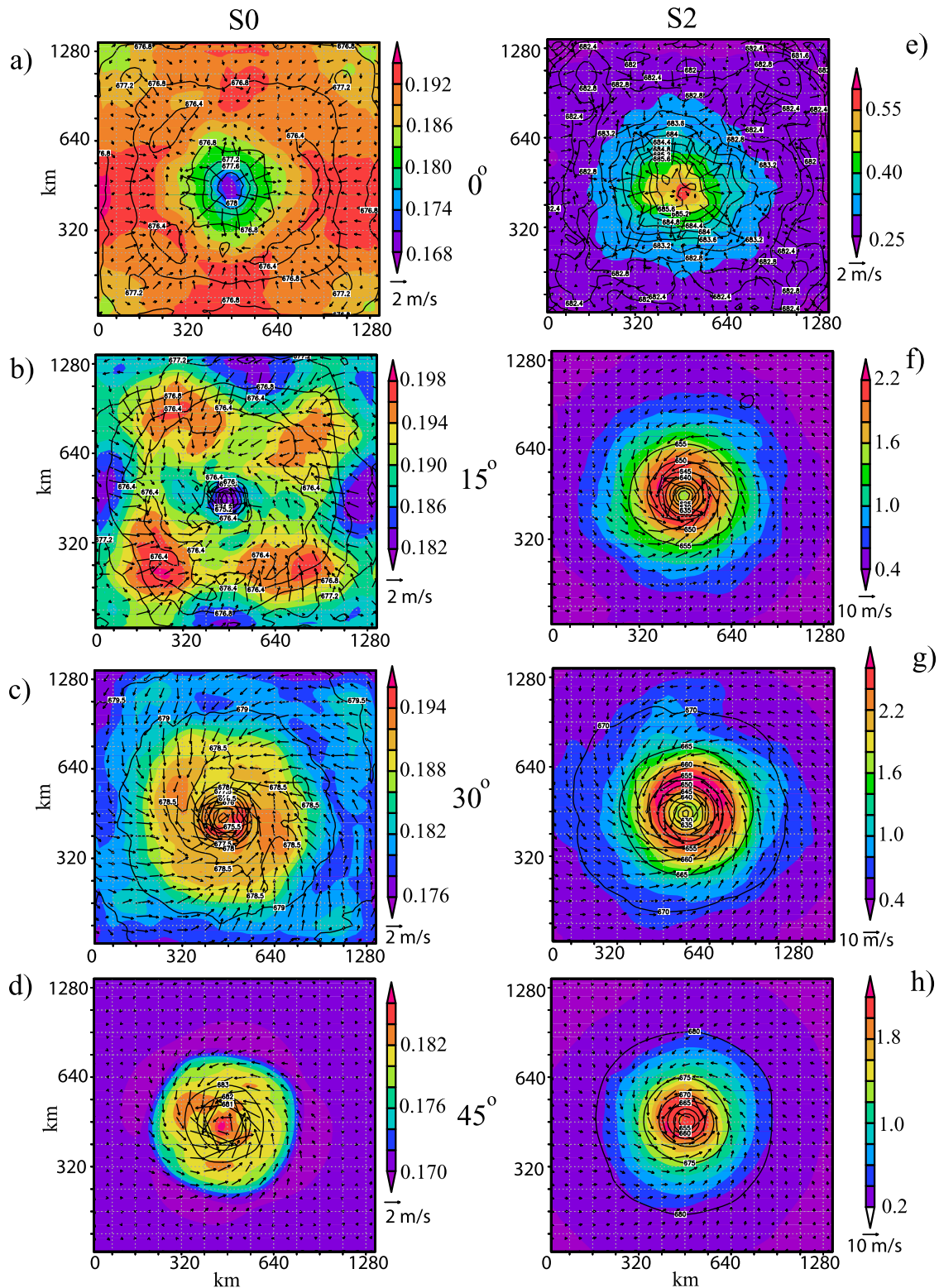


**Figure 6.** The grid 2 dust field (color shaded) late in the afternoon of the third sol is consistent with the pressure (contoured) and wind fields (vectors). In S0, where no lifting is permitted, the initial  $\tau = 1$  perturbation decays to just under  $\tau = 0.2$  at all latitudes. However, there is an increasing organizational impact on the dust as latitude increases. In S2, the extratropical cases all show roughly a twofold increase in dust opacity from the initial condition and are much more horizontally extensive. Note also the change in wind vector scale for these cases. In the equatorial case, the dust opacity decays more slowly than S0, indicating that dust lifting is active, but the radiative feedback to the dynamics is not sufficient to maintain the disturbance.

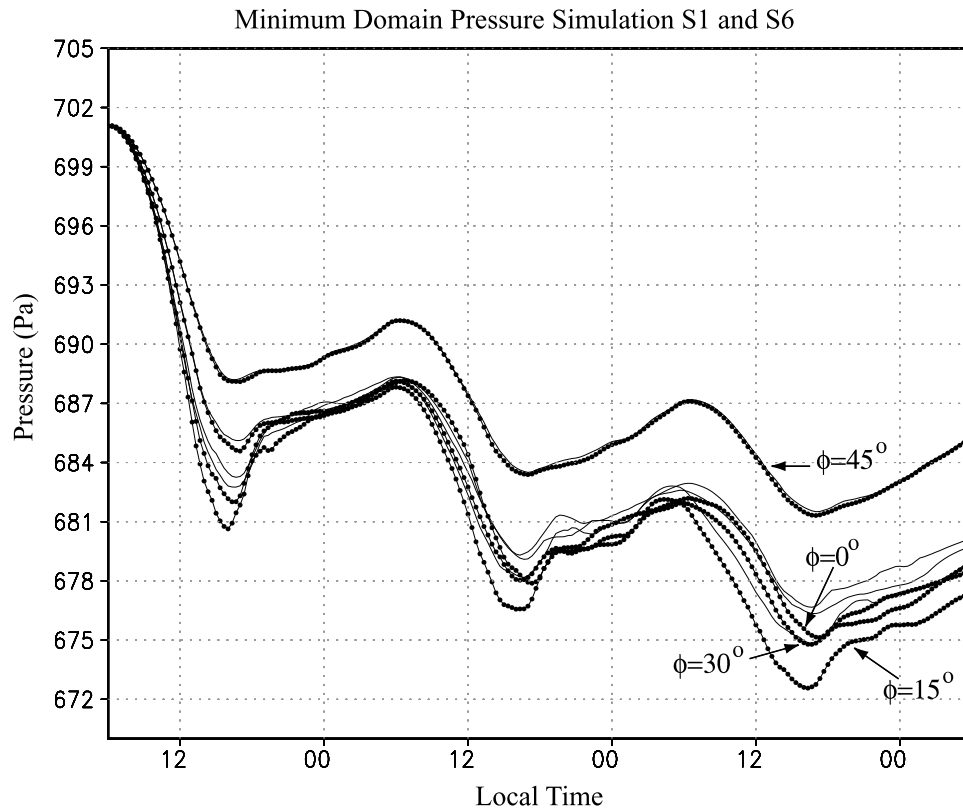


**Figure 7.** Increasing the dust-lifting efficiency can increase the strength of the circulation. In order for changes in efficiency to have an effect, the dust-lifting threshold must be exceeded. At  $45^\circ$  there is little difference between S6 and S1 because the winds are too weak to initiate much lifting. The  $15^\circ$  S1 case had the strongest winds and shows the greatest effect when combined with the favorable solar forcing and coriolis force. The equatorial and  $30^\circ$  case are similar. Both show a slight increase in strength in S6, but the overall effect is small, especially compared to changes associated with the dust-lifting threshold. Solid lines represent S1 and dotted lines S6. The S1 data are as in Figure 1.

Qualitatively, regions with limited sand would have high thresholds owing to limitations on the saltation process. Locations with indurated or cemented sand and dust would also have a high threshold. Alternatively, locations with a small surface roughness and a broad size distribution of sand and dust are likely to have low thresholds.

[34] The 1 mN threshold used in S2 is probably too low for most locations on Mars, while 14 mN may be more typical. However, there are almost certainly places where dust is lifted relatively easily, and a comparison of S0 and S2 show, that all other things being equal, these locations are more likely to produce a disturbance that amplifies.

[35] The effect of changing the dust-lifting efficiency factor is explored in S6, which is identical to S1, except that  $\alpha = 0.01$ . S1 was very similar to S0 because the winds seldom exceeded the lifting threshold. However, some lifting does occur in S1, and S6 tests whether having very efficient lifting sporadically and at limited locations is sufficient to initiate a positive feedback.

[36] The results from S6 (Figure 7) indicate a small positive feedback. Pressure is slightly lower, winds are slightly stronger (not shown), and dust optical depth is slightly greater compared to S0 or S1 (not shown). However, the differences are very minor. The  $15^\circ$  case shows the most differences because it has the strongest winds and

most often exceeds the lifting threshold. This allows the increased efficiency to have a greater effect. It is likely that if the dust-lifting threshold was lowered and the efficiency factor was raised, there might have been a greater effect at higher latitudes. The reduced impact at the equator is due to the inability to organize a balanced circulation with strong winds.

[37] To better understand the importance of the dust-lifting threshold and efficiency parameters in controlling the feedback process, over two dozen two-dimensional simulations covering a wide range of these parameters were conducted. This number of simulations is not practical in three dimensions. The 2-D simulations differ from the 3-D in a number of ways besides dimensionality. First, there is no coriolis force, so geostrophic adjustment processes are not possible. Second, there is no solar cycle. Solar insolation is fixed at a value corresponding to noon at the equator. Third, the simulations are only run for  $\sim 12$  h. Fourth, only a single 2000 km grid with 1-km horizontal spacing is used. The initial dust perturbation has the same optical depth ( $\tau = 1$ ) and has the same horizontal (10 km) and vertical dimension ( $\sim 200$  m) as in the 3-D simulations. The results from these experiments are shown in Figure 8.

[38] In the 2-D experiments, dust-lifting parameters have a large impact on the existence and strength of the feedback

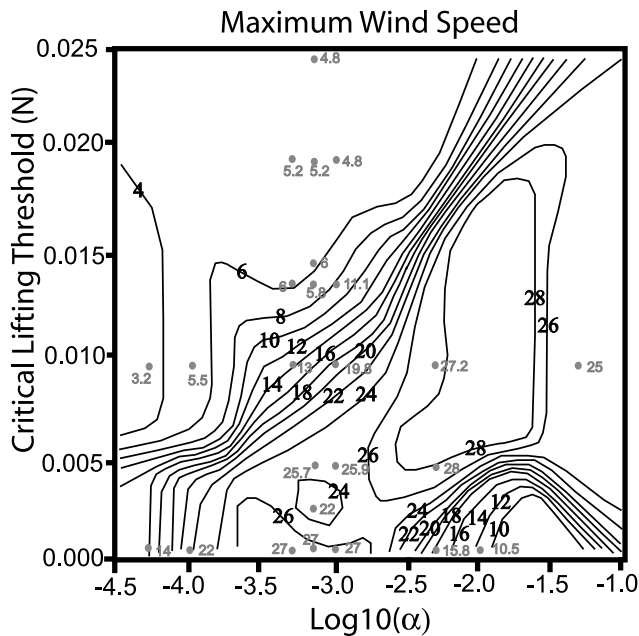


**Figure 8.** Results from the two-dimensional model simulations shows that both the dust-lifting threshold and the dust-lifting efficiency can have a large impact on the feedback. Maximum low-level wind speed in  $\text{m s}^{-1}$  is contoured. Gray dots and gray numbers show data points from simulation.

process. This is almost certainly amplified in large part by the constant and large imposed solar forcing. Optimal positive feedback occurs for moderate lifting thresholds and high lifting efficiency. This scenario allows for a

reasonable amount of dust lifting in the domain, and places relatively large amounts of dust into the atmosphere at those locations. This scenario also demonstrates that changes in lifting efficiency can modulate the feedback process, as long as dust is lifted. When the efficiency is low, regardless of the lifting threshold, the feedback is limited. This reflects that the feedback process requires dust in the atmosphere. Lifting dust alone is not sufficient; the amount of dust lifted is also important. Likewise, when the threshold is very high, there is little feedback because too little dust is lofted into the atmosphere. When the threshold is low and the efficiency is high, feedback is reduced. This may seem counterintuitive at first. The parameter settings in this case result in lots of dust being lifted everywhere, and the horizontal gradient in atmospheric heating that produces the localized warm-core low is absent. In the most extreme cases, the dust loading becomes so large that solar heating of the lower levels is reduced, which also limits development of a dynamical disturbance near the surface.

### 3.3. Effect of Background Atmospheric Thermal Structure

[39] Simulations S0 through S3 are all initialized with a 170 K isothermal background state. Simulations S4 and S5 investigate the effect of different thermal structures on the feedback process. A warmer isothermal state (215 K) and a sunrise temperature profile extracted from a realistic meso-scale simulation [c.f. Rafkin and Michaels, 2003] are used to initialize the model for simulations S4 and S5, respectively. The low-lifting threshold parameter from S2 is used in these cases since the feedback process signal is strong, and any modulation of this signal by changes in thermal structure should therefore be easier to detect.

[40] There are two striking results from the thermal structure experiments (Figure 9). The first is that both S4

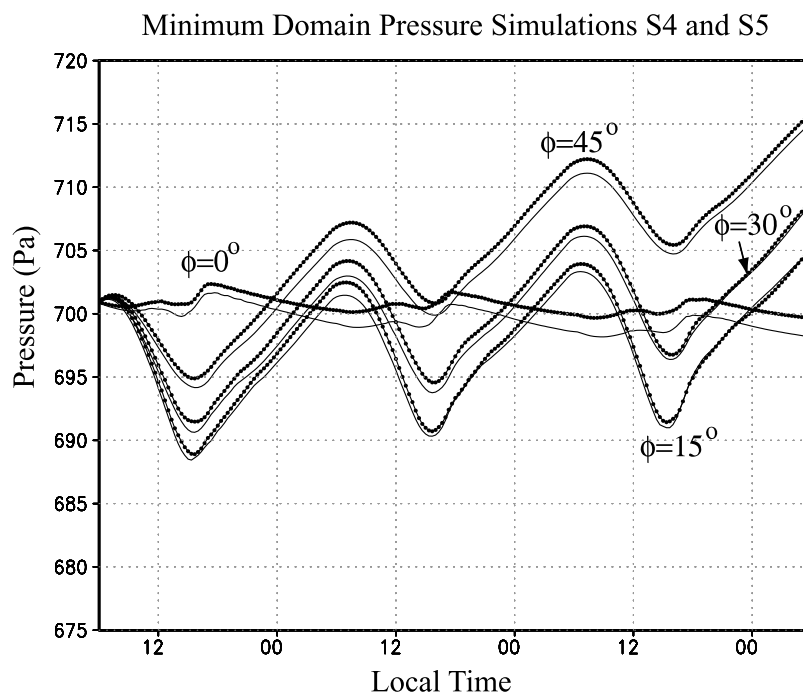


**Figure 9.** Atmospheric thermal structure has a strong influence on the amplitude of the feedback. S5 data are shown by the solid line. S6 data are shown by the dotted line.

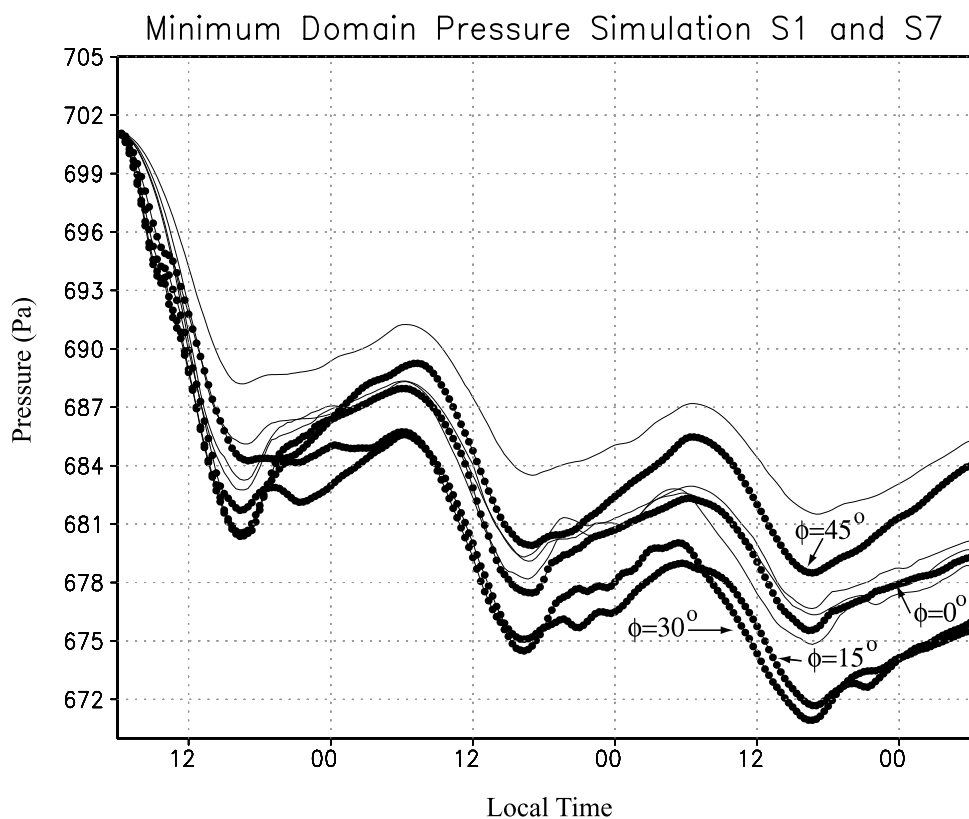


**Figure 10.** Increasing the size of the initial dust perturbation from 10 to 50 km results in deeper systems for all latitudes. However, the positive feedback in the larger perturbation scenario does not appear to be substantially greater than the smaller perturbation after the first sol. Although the system is deeper, the pressures are not falling at any greater rate than in the smaller perturbation case. Solid lines are S1 data as indicated in Figure 1, and dotted lines indicate S7.

and S5 produce weaker circulations than the 170 K isothermal cases. The second is that for a given latitude, the results from the 215 K isothermal case and the realistic temperature case are nearly indistinguishable in terms of circulation strength. The overall trend of increasing temperature in both simulations is also of note, and represents a hydrostatic response to net cooling within the domain from the warm initial conditions.

[41] From a purely qualitative viewpoint, the greater the lapse rate between the surface and the top of the circulation, the stronger the circulation. In all cases, the near-surface air is rapidly heated, but to roughly the same temperature regardless of the initial condition. However, the higher levels of the atmosphere are less susceptible to the heating, resulting in a very steep lapse rate for the 170 K isothermal case. The lapse rate is less steep in the 215 K isothermal case, and, as it turns out, is nearly the same as in the realistic temperature profile. The importance of the thermal structure on the energetics of the disturbance is further explained in section 4.

### 3.4. Effect of Initial Dust Perturbation Size

[42] On the basis of Rossby Radius of Deformation arguments previously discussed, a larger initial disturbance will be more likely to produce a balanced circulation, all other things being equal. This does not necessarily imply that the feedback mechanism will be stronger, although that

turns out to be the case; the feedback magnitude is tied to the development of a balanced circulation, which is easier to develop if the initial disturbance is larger.

[43] Disturbances much smaller than the Rossby Radius of Deformation are unlikely to achieve balance regardless of the other factors. At the equator, the Rossby Radius of Deformation is infinite, and growth through the feedback mechanism is not favored. But, from  $15^\circ$ – $30^\circ$ , a 10 km initial disturbance is shown to be sufficiently large enough to establish a strong feedback process under some conditions (e.g., S2). Furthermore, if the solar forcing remained unchanged, the same initial size disturbance would exhibit even stronger feedback at higher latitudes owing to the decrease in the  $\lambda_R$ . In reality, the solar forcing does change with latitude, and so a larger initial disturbance is required at higher latitudes in order to overcome the decrease in energy input. At some point, this becomes a losing proposition, and the feedback mechanism will become completely inefficient at high latitudes regardless of size.

[44] Even in the absence of a positive feedback process, a larger initial dust perturbation should result in a deeper and more intense circulation, all other things being equal. S7 is similar in design to S1, except that the initial size of the disturbance is 50 km rather than 10 km. The results from S7 are close to S1 (Figure 10). The larger initial disturbance does produce a slightly more intense circulation, but it is still unable to produce winds that lift much dust. Therefore,

initial size has an impact, but it becomes increasingly important if the increased perturbation allows for the initial disturbance to cross the lifting threshold. Note that although the resulting disturbance in S7 is deeper at all latitudes after the first sol compared to S1, the amplitude of the positive feedback is not obviously larger; the rate of decrease of pressure in both S1 and S7 is virtually identical. As in the case of increased lifting threshold, the limited dust lifting limits the potential increase in feedback even as other factors become more favorable.

#### 4. Energetics and Analogy to the Hurricane Feedback Process

[45] The relationship between the lapse rate and strength of the circulation is analogous to the relationship between the sea surface temperature and exhaust temperature control of hurricanes, as proposed in the Wind-Induced Sensible Heat Exchange (WISHE) hypothesis [Emanuel, 1986, 1991] and not unlike the heat engine theory proposed by Rennó and Ingersoll [1996] for convective vortices. In the WISHE hypothesis, near-surface air flowing toward the center of the hurricane gains entropy via water vapor flux at the ocean surface while undergoing isothermal expansion at a temperature near the sea surface temperature. Within the hurricane eye wall the moist air then ascends adiabatically (in the moist sense) and is exported horizontally in the upper level anticyclone, also adiabatically. The excess entropy is lost gradually and nearly isothermally through radiation during slow descent in the upper troposphere. Finally, the air descends (nearly adiabatically) back to the surface far from the vortex center to complete the circuit. These paths closely represent the isothermal and adiabatic legs of a Carnot cycle, with the efficiency of the hurricane engine being proportional to the input surface temperature and output temperature aloft. The work done is balanced by a frictional loss of energy that takes place primarily at the surface. As the input temperature increases, greater frictional loss is required for steady state conditions. This is accomplished by increasing surface winds (which are proportional to the pressure gradient). However, increasing the surface winds (by decreasing the central pressure) also increases the water vapor flux, which further increases the entropy of the system. The increase in entropy results in more work done by the hurricane that must be balanced by a further increase in wind speed, a concomitant increase in frictional loss, a decrease in pressure, and an increase in entropy input from increased water vapor flux.

[46] It is worthwhile to note how structurally similar many of the simulated dust disturbances are to tropical cyclones (Figure 11). Both are warm-core low pressure systems with maximum pressure perturbations at the surface. Both are characterized by quasi-balanced circulations (except for the equatorial cases) with low-level radial inflow toward the center, strong upward vertical velocity in an eye wall just outside the center of the circulation, and descending air in the eye of the storm. In the case of hurricanes, the descending air creates a visible eye owing to adiabatic warming and drying. This is not the case for these dust storms, as dust mixing ratio is not sensitive to temperature. However, dust does gravitationally settle out, and the downward motion at the eye tends to create a minimum

in dust optical depth. During the afternoon, when the atmosphere is convecting, the dust storm may develop spiral arm bands, which are organized updrafts aligned with the mean wind, as described by Michaels and Rafkin [2004]. At night, the air becomes stable and quasi-laminar, unlike a hurricane, and more uniform flow develops in place of the spiral arms. Horizontal wind speed is at its absolute maximum at the eye wall and local maxima collocated with the spiral arms. Updrafts in the dust storm are also collocated with the arm bands and are strongest at the eye wall. Aloft, both circulations are characterized by anticyclonic outflow and positive pressure perturbations (not shown).

[47] Unlike hurricanes, the inflow into a dust disturbance is not isothermal (Figure 12). In hurricanes, water vapor flux into the atmosphere represents a latent heating that is not realized until the adiabatic ascent within the eye wall, and thus the near-surface air remains near the temperature of the ocean. In dust storms, an injection of dust into the atmosphere provides an almost instantaneous heating term. Even so, once near the core of the dust storm, the air does rise nearly adiabatically and is expelled at a level of near-neutral environmental thermal buoyancy. This air then radiatively and nearly isothermally loses entropy and dust as it ultimately descends to complete the cycle. Thus, with the exception of the anisothermal surface leg of a dust storm, there is similarity to the WISHE hypothesis for hurricanes.

[48] Although the dust heating in dust storms is not latent, there is still a net increase in entropy for an air parcel as it moves from the periphery of the vortex toward the center. Work is being done, and for a balanced circulation, it must be balanced by frictional loss, primarily at the surface. If the work is greater than the frictional energy loss, then the system gains strength. As with hurricanes, the frictional loss is realized by increased surface wind speeds (resulting from a decrease of central pressure), which may further increase the flux of dust into the atmosphere. When hurricanes move over land or cooler water, the latent flux is eliminated or reduced, and the hurricane intensity diminishes. Likewise, dust storms that move over regions with limited dust will also lose strength.

[49] The lack of an isothermal surface leg along a streamline of the dust storm makes the analytical integration of work along such a streamline difficult, and it is therefore not a simple matter to relate the thermodynamics to the kinematic field as was done by Emanuel [1986]. Figure 12 shows that the increase in temperature along the surface is tied directly to the dust mixing ratio. However, because of the nature of thermodynamic cycles, we may imagine that the lifted dust does not cause heating until it reaches the center of the circulation. This then allows a direct isothermal integration along the surface trajectory from the periphery to the center of the circulation, and dust is carried as a latent contribution to entropy similar to the latent water vapor term ( $ds = C_p \ln T - R d \ln p + L_v q / T$  is the change of entropy). Without the added heating from dust, air flowing along the surface would expand nearly isothermally, staying at a nearly constant temperature related to the surface temperature.

[50] The structural and dynamical similarity between the simulated disturbances and hurricanes suggests it is perhaps reasonable that the dust storms behave as a Carnot engine

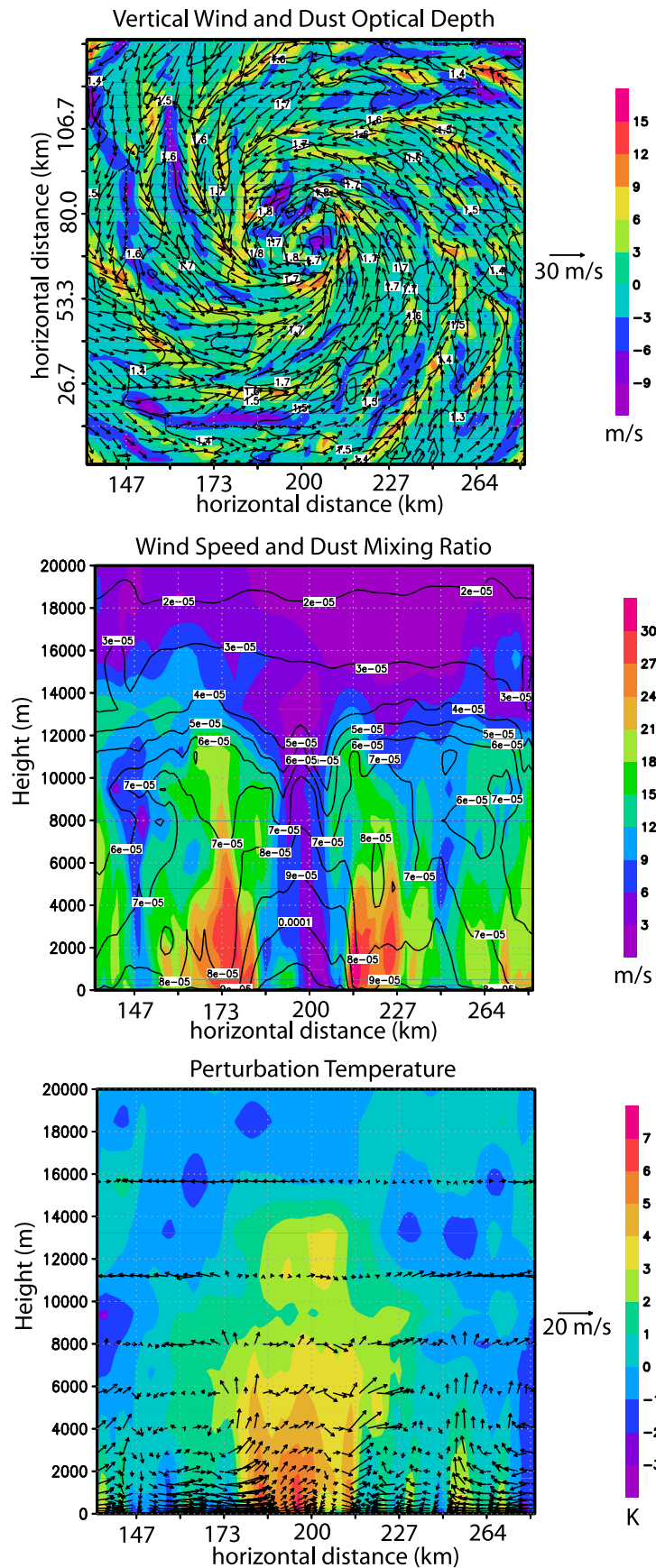
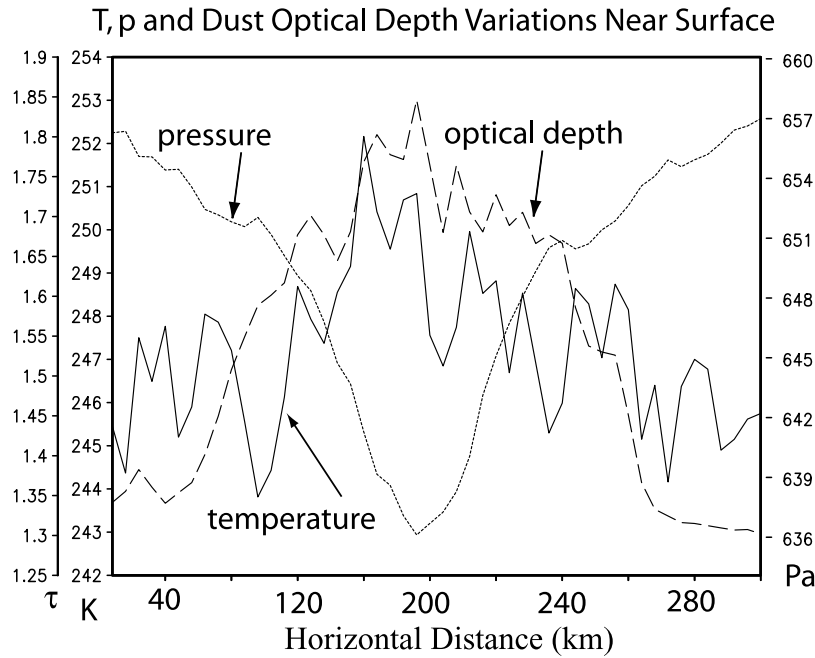


Figure 11



**Figure 12.** The trace of meteorological parameters through the storm at the surface show that temperature is maximum at the center and is strongly correlated with atmospheric dust loading. Air traveling toward the center of the vortex will undergo expansion as the pressure falls. Data are taken from grid 2 of the 30° S2 simulation.

with an intensity that can be tied to input and exhaust temperatures, as in hurricanes. For hurricanes, the efficiency is given by

$$\varepsilon = \frac{T_s - T_o}{T_s}, \quad (3)$$

where  $T_s$  is the sea surface temperature and  $T_o$  is the exhaust temperature (or output temperature) at the top of the storm. This efficiency represents the fraction of latent energy and pressure work that is converted to mechanical energy in the system as airflows from the periphery to the low pressure at the surface. As an analog, we may consider the dust storm efficiency to be the fraction of energy and pressure work that is converted to mechanical energy of the system, but rather than the acquired energy being latent, it is realized nearly immediately through solar heating of lifted dust. And, just as the latent energy in a hurricane is proportional to the amount of water evaporated into the air, the amount of heating in the dust storm is proportional to the amount of dust lifted into the atmosphere.

[51] The decrease in intensity between the S2 and S5 or S6 now makes sense in the context of a Carnot engine (Figure 13). The input temperature in S2 gradually rises in time as the 170 K initial state warms, but so does the output

temperature. The greatest difference between the two temperatures ( $\Delta T \sim 50$  K) occurs during the warmest part of the afternoon and corresponds to an efficiency of about 22%. At night, the input temperature in S2 is still warmer than the output temperature by about 15 K. In contrast, the S5 and S6 simulations have a maximum  $\Delta T$  of  $\sim 30$  K corresponding to an efficiency of about 14%. However, the difference in peak efficiency is not the only factor that explains the differences. At night, the input temperature in S5 and S6 is colder than the output temperature. When this happens, the Carnot engine runs in reverse, and extracts mechanical energy from the system; the system spins down. Finally, because of the larger lapse rate in S2, the system is also deeper than in S5 and S6 ( $\sim 12$  km versus  $\sim 8$  km), there is greater adiabatic cooling of the updraft at the core of the system, and the system exhausts at colder, higher altitudes.

[52] The WISHE hypothesis and the WISHE-like hypothesis for Martian dust storms does not explain how rotational disturbances might develop, only how such a preexisting system might amplify. However, rotation can be initiated via the well understood process of geostrophic adjustment. An initial, incipient quasi-dynamically balanced vortex is required a priori so that the surface wind speed is related to a radial pressure gradient. WISHE can be thought to operate once an incipient vortex is present.

**Figure 11.** The structure of the strongest dust storms resembles that of a hurricane. In the top, spiral arm bands are collocated with the strongest vertical velocity at 2 km above ground level (shaded) and with an increase in dust opacity (contoured). Vertical cross sections show maximum winds in an eye wall (shaded in middle) and an eye structure in the dust field (contoured in middle). Perturbation temperatures (shaded bottom) shows that the dust storm is warm core, and wind vectors show the low-level storm inflow, upper level outflow, upwelling in eye wall and spiral arm bands, and downwelling in the eye. Data are taken from grid 4 of the 30° S2 simulation.

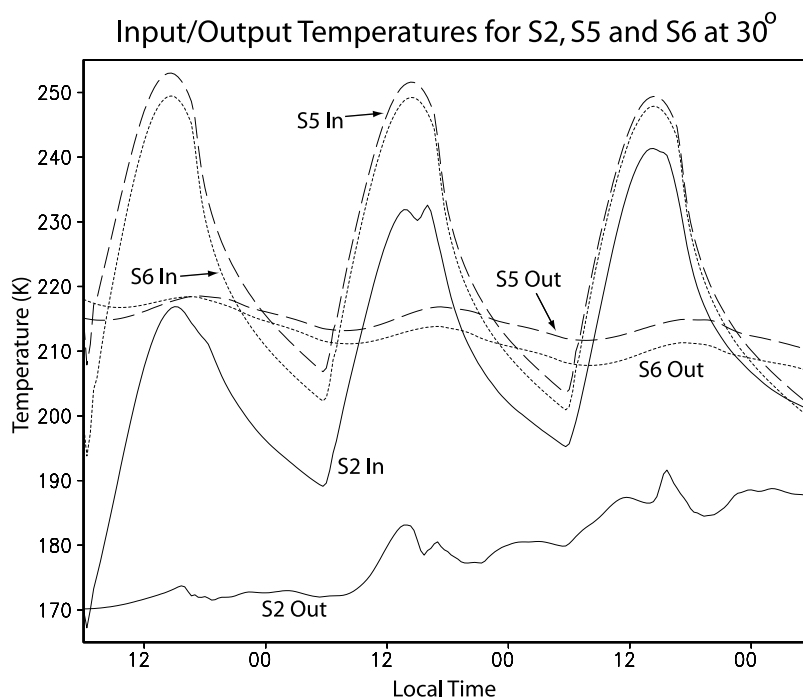


**Figure 13.** Dust storms may operate like Carnot engines. If so, the energetics are controlled by the input and output temperatures. The efficiency of S2 is greatest because of the relatively large difference between the input and output temperatures. S5 and S6 are less efficient, and because they have similar input and output temperatures, the results from these two simulations are comparable. Also note that in the cases where the input temperature is less than the output, the engine runs in reverse and extracts mechanical energy from the system.

[53] WISHE development of hurricanes is latitudinally confined to subtropics. The requirement of a balanced circulation component precludes substantial amplification at very low latitudes. At high latitudes, WISHE is not efficient for hurricanes because the sea surface temperature is too low. WISHE intensification of the simulated dust storms is similarly latitudinally confined, with the coriolis force limiting the low-latitude extension and solar heating limiting the high latitudes.

[54] One of the most important factors that can limit hurricane strength and growth is wind shear, typically associated with a baroclinic environment. Wind shear disturbs the symmetry of hurricanes and disrupts the dynamics behind the Carnot cycle. Extrapolating this result to Mars dust storms suggests that regions with strong wind shear would not be favorable for the development of dust storms similar to the ones simulated in this paper. Frontal dust storms and perhaps storms originating along the polar cap boundaries are examples of storms that are not good fits to the feedback paradigm discussed here, although it is possible that other or similar feedback mechanisms may be involved. Atmospheric dust loading is thought to have an impact, for example, on baroclinic storm intensity [Barnes, 1984].

## 5. Observations

[55] To date, no obvious dust “hurricanes” with the structure shown in Figure 11 have been unambiguously observed. Rafkin *et al.* [2002] presented a modeling study of

a spiral dust and water ice cloud on the summit of Arsia Mons, but found that dust loading had little impact on the circulation. This finding should be reinvestigated with the more sophisticated CARMA dust and radiation model.

[56] Closer inspection of Figure 11 shows that the hurricane-like dust structure might be very difficult to observe from orbit, even with very careful analysis of the available imagery. The simulated spiral arm bands are only slightly enhanced in opacity; the contouring interval in Figure 11 makes the bands stand out much more than they would in a visible image. From orbit, the simulated dust storms would likely appear as opaque, quasi-circular disturbances with embedded connective looking features. Such disturbances have been observed (Figure 14). With relatively featureless dust structures, and without direct measurement of winds, it would be very difficult to establish any circulation in these imaged disturbances. Therefore, while frontal or polar cap dust storms do not fit the paradigm of the storms presented in this paper, there are numerous other disturbances that cannot be easily excluded from the feedback paradigm presented herein.

## 6. Summary and Conclusions

[57] Numerous idealized simulations were presented to investigate the potential for a positive radiative-dynamic feedback mechanism for the maintenance and growth of dust disturbances on Mars. Under some conditions, a strong positive feedback was found. The thermodynamics and dynamics of the simulated dust storms were similar in many

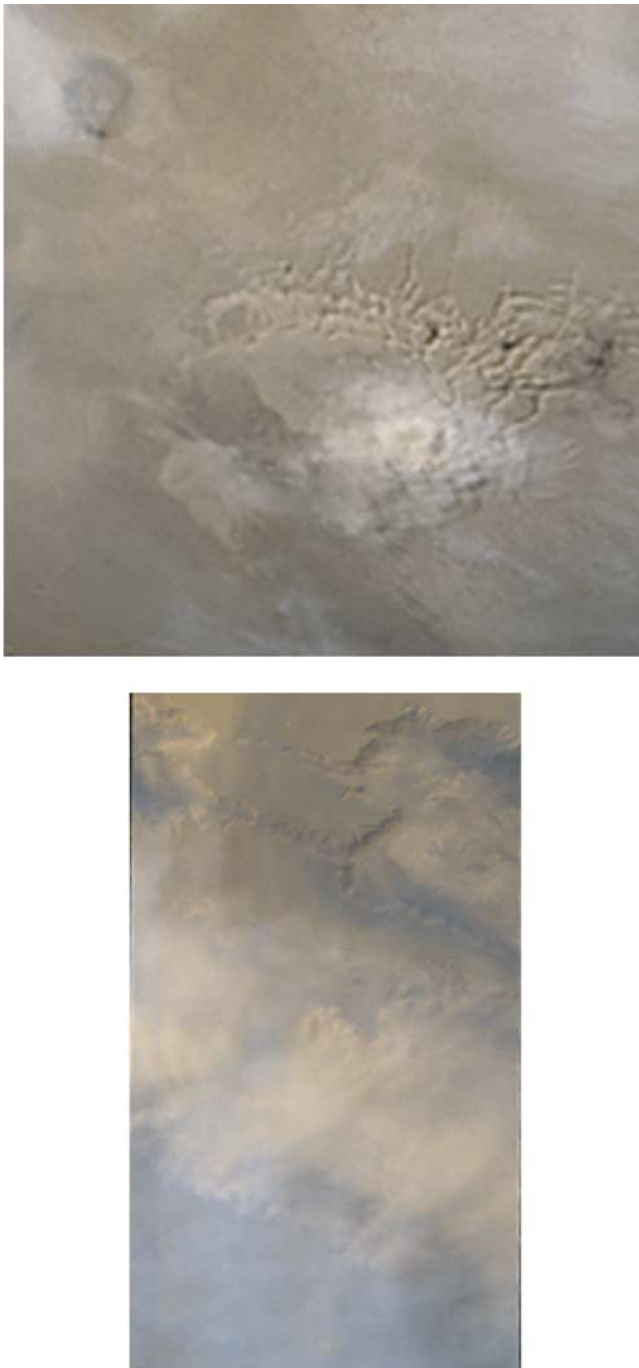


**Figure 14.** Some dust storms may be strongly influenced by the proposed positive radiative-dynamic feedback mechanism. These Mars Orbiter Camera (MOC) images show examples of storms that have no obvious causes such as baroclinic disturbances or polar cap circulations. The storms have a convective appearance and the dust lifting is localized. The top image (MOC2-366) is centered on Noctis Labyrinthus, and the bottom is centered on Valles Marineris (MOC2-130b). Confirming the existence of the positive feedback mechanism through imagery may be difficult because many of the predicted characteristics may not be discernable in the imagery. (Image from NASA/JPL/MSSS.)

respects to hurricanes. However, many of the structures may be difficult to observe from orbit. Like hurricanes, the conditions that favor a positive feedback are best explained by a combination of the geostrophic adjustment process and a WISHE-like Carnot engine cycle.

[58] The geostrophic adjustment process favors locations with strong solar forcing, and a nonnegligible coriolis force. These conditions are maximized in the subtropics, and might be further enhanced by seasonal shifts toward the summer pole driven by solar insolation. Increasing coriolis force (or equivalently, increasing latitude) makes for a dynamically more efficient circulation that can retain more of the solar energy input as a balanced circulation. However, the increasing dynamic efficiency as a function of latitude is tempered by a decrease in solar insolation. The size of the initial disturbance is also important, as the fraction of gravity wave energy radiated away is inversely proportional to the size of the disturbance. Larger initial disturbances are dynamically more efficient. The impact of increasing the size of the disturbance is only significant if the dust-lifting threshold is exceeded. Dust must necessarily be mobile for the feedback process to exist; without additional lifted dust, the initial system disperses the dust and weakens. Locations where dust can be easily lifted are favored, as an initial system requires a relatively lower wind speed to initiate the feedback process. Alternatively, the feedback process can occur even if dust-lifting thresholds are moderate if the dust-lifting efficiency is relatively high. However, even with a high lifting efficiency, the circulation must lift dust, and this requires that the system exceed some critical wind speed threshold that depends on the properties of the surface.

[59] Atmospheric thermal and kinematic structure also play a very important role in determining the magnitude of the feedback. On the basis of the hurricane analogy, barotropic atmospheric environments are favorable regions for development, while baroclinic, sheared environments are less favorable. Steep lapse rates favor development because they increase the difference between input and output temperatures. The increase in system depth associated with the steep lapse rates further enhances this effect because the system exhausts air at a higher altitude where temperatures are typically colder. If the upper levels are too warm, the system can operate as a reverse Carnot engine during the night when surface temperatures become colder than the air aloft.

[60] Steep lapse rates might be found under a variety of conditions. Cold air coming off the polar caps during the late spring and early summer might produce steep lapse rates as the near-surface air is strongly heated, but these regions also probably have strong wind shears that might disrupt the feedback process. Regions of elevated topography with respect to surrounding areas would also generally produce steep lapse rates as the near-surface temperature is not closely tied to elevation but rather to thermal inertia, albedo, and solar insolation. Southern latitude regions near the hemispheric topographic dichotomy, or at the rim of Hellas are examples of regions that might benefit from this effect. Low thermal inertia and low albedo (e.g., dark sands) would also produce the strongest low-level heating and tend to increase the lapse rate. Although higher surface elevations may produce favorable lapse rates, the decreasing density with altitude could limit the dust lifting. Higher

elevations produce an effect analogous to increasing the wind stress lifting threshold.

[61] The positive radiative-dynamic feedback described in this paper may be able to explain the growth of disturbances not clearly linked with known causal mechanisms, such as baroclinic systems and polar cap circulations. This might include some disturbances that lead to regional or larger dust storms. It might also explain how such disturbances can be maintained over many sols. In order for a positive feedback to occur, conditions have to be just right, and this may explain why most dust storms do not grow explosively and instead dissipate within one sol.

[62] A focused observational study is needed to search for disturbances that might be driven by the proposed radiative-dynamic feedback process. Furthermore, a detailed GCM and mesoscale modeling study that focuses on evaluating regions that would be climatologically favored for dust storm feedback would be valuable, especially if the results are correlated with observations. A capable meteorological station, or ideally a network of stations with long lifetimes, would be instrumental in establishing the structure within dust storms, and in better understanding the processes operating to produce, maintain, and amplify these systems. Satellites with synoptic coverage (e.g., geosynchronous rotation) capable of monitoring storm lifecycles would also be beneficial.

[63] **Acknowledgments.** Support for this research was provided by NASA under Mars Fundamental Research Program grant NNG05GM09G. The author is extremely grateful for the insightful discussions on the subject matter by Jude Sabato, Timothy Michaels, and Erika Barth, all of whom also provided helpful comments on the manuscript. The comments and criticisms provided by the anonymous reviewer were appreciated and greatly improved the quality of this paper. Finally, the editorial services provided by Jeannette Thorn are also very much appreciated.

## References

- Barnes, J. R. (1984), Linear baroclinic instability in the Martian atmosphere, *J. Atmos. Sci.*, *41*, 1536–1550, doi:10.1175/1520-0469(1984)041<1536:LBIITM>2.0.CO;2.
- Basu, S., J. Wilson, M. Richardson, and A. Ingersoll (2006), Simulation of spontaneous and variable global dust storms with the GFDL Mars GCM, *J. Geophys. Res.*, *111*, E09004, doi:10.1029/2005JE002660.
- Carrier, G. F. (1971), The intensification of hurricanes, *J. Fluid Mech.*, *49*, 145–158, doi:10.1017/S0022112071001976.
- Emanuel, K. A. (1986), An air-sea interaction theory for tropical cyclones. Part I: Steady-state maintenance, *J. Atmos. Sci.*, *43*, 585–604, doi:10.1175/1520-0469(1986)043<0585:AASITF>2.0.CO;2.
- Emanuel, K. A. (1991), The theory of hurricanes, *Annu. Rev. Fluid Mech.*, *23*, 179–196, doi:10.1146/annurev.fl.23.010191.001143.
- Ghan, S. J. (1989), Unstable radiative-dynamical interactions. Part I: Basic theory, *J. Atmos. Sci.*, *46*, 2528–2543.
- Gierasch, P. J., and R. M. Goody (1973), A model of a Martian great dust storm, *J. Atmos. Sci.*, *30*, 169–179, doi:10.1175/1520-0469(1973)030<0169:AMOAMG>2.0.CO;2.
- Gierasch, P. J., A. P. Ingersoll, and R. T. Williams (1973), Radiative instability of a cloudy planetary atmosphere, *Icarus*, *19*, 473–481, doi:10.1016/0019-1035(73)90074-2.
- Haberle, R. M., C. B. Leovy, and J. B. Pollack (1982), Some effects of global dust storms on the atmospheric circulation of Mars, *Icarus*, *50*, 322–367, doi:10.1016/0019-1035(82)90129-4.
- Kahre, M. A., J. R. Murphy, and R. M. Haberle (2006), Modeling of the Martian dust cycle and surface dust reservoirs with the NASA Ames general circulation model, *J. Geophys. Res.*, *111*, E06008, doi:10.1029/2005JE002588.
- Michaels, T. I., and S. C. R. Rafkin (2004), Large eddy simulation of atmospheric convection on Mars, *Q.J.R. Meteorol. Soc.*, *130*, 1251–1274, doi:10.1256/qj.02.169.
- Michaels, T. I., A. Colaprete, and S. C. R. Rafkin (2006), Significant vertical water transport by mountain-induced circulations on Mars, *Geophys. Res. Lett.*, *33*, L16201, doi:10.1029/2006GL026562.
- Rafkin, S. C. R., and T. I. Michaels (2003), Meteorological predictions for 2003 Mars Exploration Rover high-priority landing sites, *J. Geophys. Res.*, *108*(E12), 8091, doi:10.1029/2002JE002027.
- Rafkin, S. C. R., R. M. Haberle, and T. I. Michaels (2001), The Mars regional atmospheric model: Model description and selected simulations, *Icarus*, *151*, doi:10.1006/icar.2001.6605.
- Rafkin, S. C. R., M. R. V. Sta. Maria, and T. I. Michaels (2002), Simulation of the atmospheric thermal circulation of a Martian volcano using a mesoscale numerical model, *Nature*, *419*, 697–699, doi:10.1038/nature01114.
- Rennó, N.O., and A. P. Ingersoll (1996), Convection as a heat engine: A theory for CAPE, *J. Atmos. Sci.*, *53*, 572–585, doi:10.1175/1520-0469(1996)053<0572:NCAAHE>2.0.CO;2.
- Toigo, A. D., M. I. Richardson, R. J. Wilson, H. Wang, and A. P. Ingersoll (2002), A first look at dust lifting and dust storms near the south pole of Mars with a mesoscale model, *J. Geophys. Res.*, *107*(E7), 5050, doi:10.1029/2001JE001592.
- Toon, O. B., C. P. McKay, T. P. Ackerman, and K. Santhanam (1989), Rapid calculation of radiative heating rates and photodissociation rates in inhomogeneous multiple scattering atmospheres, *J. Geophys. Res.*, *94*, 16,287–16,301, doi:10.1029/JD094iD13p16287.
- Wang, H. (2007), Dust storms originating in the northern hemisphere during the third mapping year of Mars Global Surveyor, *Icarus*, *189*, 325–343, doi:10.1016/j.icarus.2007.01.014.

---

S. C. R. Rafkin, Department of Space Studies, Southwest Research Institute, 1050 Walnut Street, Suite 300, Boulder, CO 80302, USA. (rafkin@boulder.swri.edu)